Magnetization studies in transition-metal niobates: I. $NiNb_2O_6$

I. Yaeger* and A. H. Morrish
Department of Physics, The University of Manitoba, Winnipeg, Canada

B. M. Wanklyn
Clarendon Laboratory, Oxford, England

(Received 9 July 1976)

The principal magnetic susceptibilities of $NiNb_2O_6$ were measured from ambient down to 1.4 K. At $T_N = 6.0 \pm 0.3$ K an antiferromagnetic ordering was observed. An antiferromagnetic-paramagnetic phase transition was induced by external magnetic fields parallel to the crystallographic $\vec{c}$ axis in the temperature range below T_N. The experimental results are interpreted in terms of anisotropic bilinear interactions between Ni^{2+} ions within the manifold of the ground term $^3A_2$. A two-sublattice uniaxial antiferromagnet model is used to describe the Ni^{2+} spins in the mean-field approximation. The bilinear Ni^{2+}-Ni^{2+} interactions are essentially of the exchange type with a small dipolar contribution. Along all three orthorhombic directions the ferromagnetic intrasublattice interaction is found to be stronger than the intersublattice antiferromagnetic coupling. The Ni^{2+} g tensor, taken to be isotropic, is $g = 2.4 \pm 0.1$ and the uniaxial anisotropy term $-KS_z^2$ in the effective spin Hamiltonian with $S = 1$ yields $K = 7.9 \pm 0.7$ K/spin.

I. INTRODUCTION

The transition-metal niobates MNb_2O_6 (M = Co, Fe, Mn, Ni) belong to a class of orthorhombic columbites (space group D_{2h}^{14}-$Pbcn$).[1] There are four formula units per crystallographic unit cell. The structure consists of layers of MO_6 octahedra at $x = 0$ and $x = 0.5$ which are separated by two intervening NbO_6 layers. Each M^{2+} ion is surrounded by a nearly regular octahedron of oxygen atoms. The site symmetry at the location of the M^{2+} ions is 2_y. In the notation adopted in this paper the lattice constants of $NiNb_2O_6$ are $a = 14.01$ Å, $b = 5.661$ Å, $c = 5.013$ Å.[1]

Neutron-diffraction studies made on powder samples of some of these materials indicate that the Co, Fe, and Mn niobates are antiferromagnetically ordered at liquid-helium temperatures.[2,3] A doubling of the unit cell was found to be associated with the magnetic ordering in $CoNb_2O_6$ and $FeNb_2O_6$,[3] whereas in $MnNb_2O_6$ the magnetic unit cell is identical to the crystallographic one.[3] No neutron diffraction work on $NiNb_2O_6$ has come to the attention of the present authors.

Studies of transition-metal niobates in a single-crystal form have been reported so far only on $MnNb_2O_6$,[4] and $CoNb_2O_6$.[5] In this paper, we report theoretical and experimental susceptibility studies on single crystals of $NiNb_2O_6$. Further, we elaborate on a group-theoretical analysis that is applicable to the studies of other transition-metal niobates as well. The experimental susceptibilities along the orthorhombic crystallographic axes are given in Sec. II. In Sec. III group-theory considerations are applied to the M^{2+}-M^{2+} bilinear interactions, magnetocrystalline anisotropy and the g-tensor components of the M^{2+} ions within the space group $Pbcn$. The M^{2+} spin configurations compatible with the maximal symmetry of the crystallographic space group are also derived. The analysis of the temperature dependence of the magnetic susceptibility along the principal crystallographic directions is the subject of Sec. IV. In the discussion that takes place in Sec. V the various approximations employed in the analysis and the agreement with the experimental data are evaluated.

II. EXPERIMENTAL

Single crystals of $NiNb_2O_6$ were grown using $Na_2B_4O_7$ and excess of Nb_2O_5 as flux. The contamination from this mixture was only 0.04% Na in the crystals. The mixture was placed in a platinum crucible with a closely fitted lid, held 15 h at 1250 °C, cooled at 1 °C/h to 870 °C and then moved rapidly to room temperature. The crystals (weighing a few tens of milligrams) were identified as the orthorhombic columbite phase (space group D_{2h}^{14}-$Pbcn$) from powder x-ray diffraction patterns. Their field-induced magnetization and principal susceptibilities were measured by means of a PAR vibrating sample magnetometer model FM-1. The sample was cooled by a stream of helium gas inside a metal cryostat. Constant temperatures were maintained by using a heating coil to balance the cooling effect of the helium stream. The temperature was recorded by an Au–0.03-at.%-Fe vs chromel-P thermocouple. In addition, measurements at and below 4.2 K were taken with the sample immersed in liquid helium in a glass cryostat. Below 4.2 K the temperature was controlled

by monitoring the vapor pressure over the liquid helium. The temperature in that range was measured using a calibrated Ge resistor. The reported results were compiled from (i) magnetization measurements versus temperature recorded at various fixed magnetic fields while heating or cooling the sample and (ii) curves of magnetization versus applied field recorded at fixed temperatures.

The susceptibilities along the orthorhombic crystallographic axes of $NiNb_2O_6$ are shown in Fig. 1. All three susceptibility curves peak at about $T = 6.5$ K. The antiferromagnetic ordering point however is associated with the maximum in $d\chi/dT$ at $T_N = 6.0 \pm 0.3$ K. There is a decrease in the susceptibility below T_N along the three orthorhombic axes with the sharpest decrease occurring along the $\vec{c}$ direction. In the magnetization versus field curves along the principal crystallographic axes that are shown in Fig. 2, the $\vec{c}$ direction is again singled out. Whereas the field dependence of the magnetization along both $\vec{a}$ and $\vec{b}$ axes is almost linear in the range of measurement from 0 to 19 kOe the $\vec{c}$ direction magnetization exhibits a remarkable field dependence. It is on these grounds that we conclude that the spin easy axes of the Ni^{2+} ions are either very close to or coincide with the crystallographic $\vec{c}$ axis. The field dependence of the magnetization along the $\vec{c}$ axis shown in Fig. 2 is interpreted as a field-induced phase transition from an antiferromagnetic to a paramagnetic state.

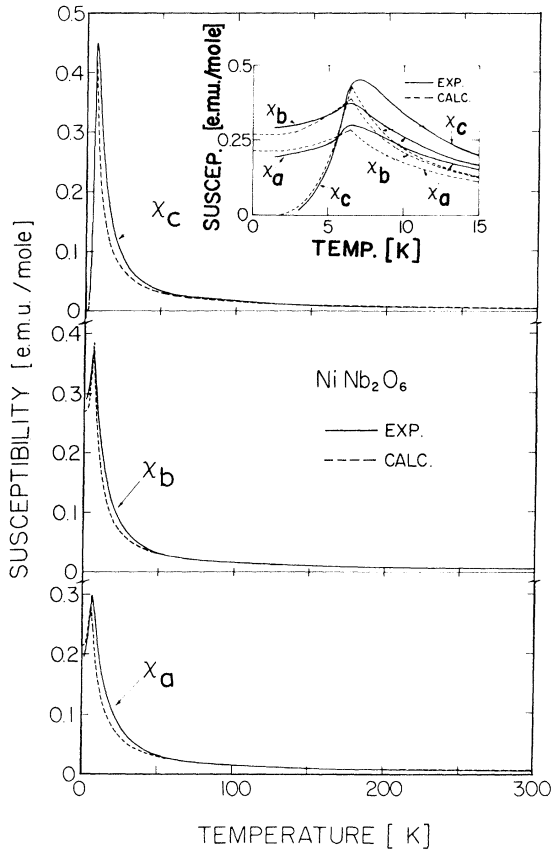

FIG. 1. Principal magnetic susceptibilities of $NiNb_2O_6$ as a function of temperature. The subscripts a, b, c refer to the orthorhombic crystallographic axes. Inset shows expanded scale at low temperatures.

III. GROUP-THEORY CONSIDERATIONS

The main purpose of the present group theoretical treatment is to derive the form of second-order magnetocrystalline anisotropy terms, the g tensor and the bilinear Ni^{2+}-Ni^{2+} interactions in $NiNb_2O_6$. Further, we obtain the Ni^{2+} spin configurations compatible with the maximal symmetry of the space group $Pbcn$. This makes the implications of the various approximations made in the analysis of the susceptibility data clearer. In the absence of neutron diffraction data, the spin configurations obtained here will also shed light on some of the possible magnetic structures of $NiNb_2O_6$ in the antiferromagnetically ordered phase including those that do not necessarily possess the full symmetry of $Pbcn$. Since the treatment is of a general nature it is applicable not only to $NiNb_2O_6$ but also to the other transition-metal niobates and to some other isostructural materials as well.

Here we shall essentially follow the method used by Bertaut[6] in which the transformation properties of the magnetic structure and the effective spin Hamiltonian under the classical symmetry

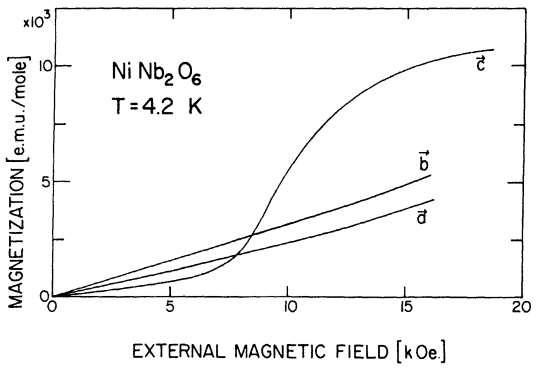

FIG. 2. Magnetization of $NiNb_2O_6$ as a function of an applied magnetic field along the orthorhombic $\vec{a}$, $\vec{b}$, and $\vec{c}$ directions at $T = 4.2$ K.

operations of the space group and time reversal are considered. We take an effective spin Hamiltonian that is bilinear in the spin components (and therefore automatically invariant under time reversal) and from its invariance under the symmetry operations of the space group the forms of magnetocrystalline anisotropy terms, the g tensor and Ni^{2+}-Ni^{2+} bilinear interaction tensors are determined.

A. Magnetocrystalline anisotropy and the g tensor

The Ni^{2+} ions occupy the 4(c) sites in the crystallographic unit cell. Their locations are (1) $0y\frac{1}{4}$, (2) $0\bar{y}\frac{3}{4}$, (3) $\frac{1}{2}\frac{1}{2}-y\frac{3}{4}$, and[1] (4) $\frac{1}{2}\frac{1}{2}+y\frac{1}{4}$ (see Fig. 3) where we estimate y to be about 0.11. In considering the effect of the symmetry operations of the space group on the Ni^{2+} spins it is sufficient to take into account only the generators of *Pbcn*. As generators of the space group we select 2_{1x} at $x\frac{1}{4}0$, 2_y at $0y\frac{1}{4}$ and $\bar{1}$ at 000. The transformation properties of the Ni^{2+} spin components under these operators are listed in Table I. It is evident that each of the generators is actually a product of two operators, one of which is acting on the sites and the other one on the spin components of the Ni^{2+} ions. Thus 2_{1x} interchanges sites 1 and 3 and also sites 2 and 4. Its total effect is illustrated by writing 2_{1x} in the form

$$2_{1x}=\begin{pmatrix}1&0&0\\0&-1&0\\0&0&-1\end{pmatrix}\cdot\begin{bmatrix}1-3\\2-4\end{bmatrix}. \tag{1}$$

Similarly,

$$2_y=\begin{pmatrix}-1&0&0\\0&1&0\\0&0&-1\end{pmatrix}\cdot\begin{bmatrix}1-1\\2-2\\3-3\\4-4\end{bmatrix},$$

$$\bar{1}=\begin{pmatrix}1&0&0\\0&1&0\\0&0&1\end{pmatrix}\cdot\begin{bmatrix}1-2\\3-4\end{bmatrix},$$

where [ ] indicates interchanging of sites. Invariance of the effective spin Hamiltonian $\mathcal{H}$ under 2_{1x}, 2_y, and $\bar{1}$ implies that $\mathcal{H}$ commutes with these operators or equivalently that the following equations hold

$$2_{1x}\mathcal{H}2_{1x}^{-1}=\mathcal{H},\quad 2_y\mathcal{H}2_y^{-1}=\mathcal{H},\quad \bar{1}\mathcal{H}\bar{1}^{-1}=\mathcal{H}. \tag{2}$$

Second-order magnetocrystalline anisotropy in the effective spin Hamiltonian has the form of "self-interaction" and will be given by

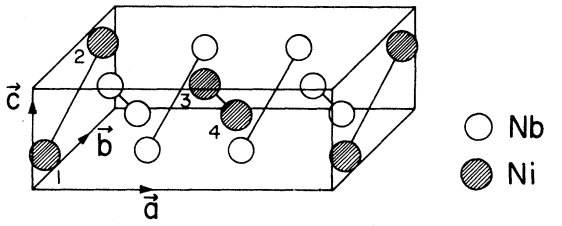

FIG. 3. Crystallographic unit cell of $NiNb_2O_6$. Ni^{2+} ions occupy the 4(c) sites at (1) $0y\frac{1}{4}$, (2) $0\bar{y}\frac{3}{4}$, (3) $\frac{1}{2}\frac{1}{2}-y\frac{3}{4}$, and (4) $\frac{1}{2}\frac{1}{2}+y\frac{1}{4}$.

$$\mathcal{H}_{an}=\vec{S}_1^t\cdot K_1\cdot\vec{S}_1+\vec{S}_2^t\cdot K_2\cdot\vec{S}_2+\vec{S}_3^t\cdot K_3\cdot\vec{S}_3+\vec{S}_4^t\cdot K_4\cdot\vec{S}_4, \tag{3}$$

where $\vec{S}_i$ is the column spin vector of ion i and $\vec{S}_i^t$ its transpose, $i=1,2,3,4$. The K_i's are 3×3 matrices. When the operator equations (2) are applied to the magnetocrystalline anisotropy term (3) one gets the matrix form of K_i $i=1,2,3,4$. In the derivation of the matrix form of K_i it is further taken into account that $\mathcal{H}_{an}$ is Hermitian and that K_i's are real and therefore symmetric. The following expressions for K_i $i=1,2,3,4$, are obtained

$$K_1=K_2=\begin{pmatrix}k_{11}&0&k_{13}\\0&k_{22}&0\\k_{13}&0&k_{33}\end{pmatrix},$$

$$K_3=K_4=\begin{pmatrix}k_{11}&0&-k_{13}\\0&k_{22}&0\\-k_{13}&0&k_{33}\end{pmatrix}. \tag{4}$$

It is evident now that the 4(c) sites, occupied by the Ni^{2+} ions, which are crystallographically equi-

TABLE I. Spin transformations in *Pbcn* [sites 4(c)].

1	2_{1x}	2_y	$\bar{1}$
S_{1x}	S_{3x}	$-S_{1x}$	S_{2x}
S_{1y}	$-S_{3y}$	S_{1y}	S_{2y}
S_{1z}	$-S_{3z}$	$-S_{1z}$	S_{2z}
S_{2x}	S_{4x}	$-S_{2x}$	S_{1x}
S_{2y}	$-S_{4y}$	S_{2y}	S_{1y}
S_{2z}	$-S_{4z}$	$-S_{2z}$	S_{1z}
S_{3x}	S_{1x}	$-S_{3x}$	S_{4x}
S_{3y}	$-S_{1y}$	S_{3y}	S_{4y}
S_{3z}	$-S_{1z}$	$-S_{3z}$	S_{4z}
S_{4x}	S_{2x}	$-S_{4x}$	S_{3x}
S_{4y}	$-S_{2y}$	S_{4y}	S_{3y}
S_{4z}	$-S_{2z}$	$-S_{4z}$	S_{3z}

valent, give rise to two types of magnetically nonequivalent sites in case of $k_{13} \neq 0$. It can be shown that the matrices K_1 and K_2 can be diagonalized by the orthogonal transformation $R(\phi)$,

$$R(\phi) = \begin{pmatrix} \cos\phi & 0 & \sin\phi \\ 0 & 1 & 0 \\ -\sin\phi & 0 & \cos\phi \end{pmatrix} \tag{5}$$

and that matrices K_3 and K_4 can be brought to the identical diagonal matrix by the transformation $R(-\phi)$ where

$$\cot(2\phi) = (k_{11} - k_{33})/2k_{13}\,. \tag{6}$$

From the relations

$$R^t(\phi)K_1R(\phi) = R^t(\phi)K_2R(\phi) = R^t(-\phi)K_3R(-\phi)$$

$$= R^t(-\phi)K_4R(-\phi) = \begin{pmatrix} k'_{11} & 0 & 0 \\ 0 & k'_{22} & 0 \\ 0 & 0 & k'_{33} \end{pmatrix}, \tag{7}$$

it follows that the two types of sites differ in the angles that the local principal axes of the g tensor make with the crystallographic axes. Although the crystallographic $\vec{b}$ axis is a principal direction of the g tensor on both types of sites, the local principal axes in the $\vec{a} - \vec{c}$ plane are symmetrically displaced with respect to the crystallographic axes (see Fig. 4).

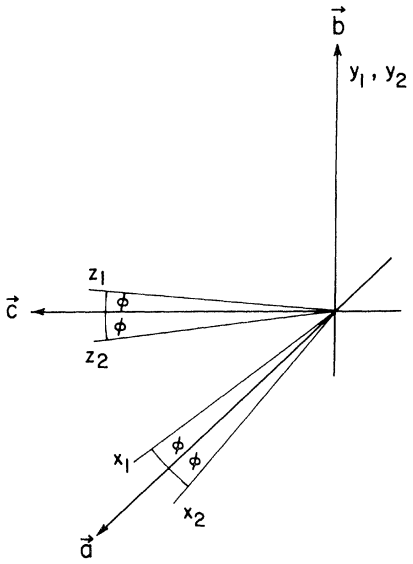

FIG. 4. Local principal axes x_i, y_i, z_i of the g tensor of magnetic ions occupying the two types of magnetically non equivalent 4(c) sites in *Pbcn*. $\vec{a}$, $\vec{b}$, and $\vec{c}$ mark the orthorhombic crystallographic axes.

B. Ni^{2+}-Ni^{2+} bilinear interactions

The bilinear interactions between spins on the Ni^{2+} sublattices are represented in the effective spin Hamiltonian by the term

$$\mathcal{H}_{\text{int}} = \sum_{i,j=1}^{4} \vec{S}_i^{\,t} \cdot D_{ij} \cdot \vec{S}_j\,, \tag{8}$$

where D_{ij} is the 3×3 interaction matrix between a spin on sublattice i and one on sublattice j. As $\mathcal{H}_{\text{int}}$ is Hermitian and the D_{ij} matrices are real it follows that

$$D_{ij}^t = D_{ji}\,, \quad i,j = 1,2,3,4\,. \tag{9}$$

The forms of the D_{ij} matrices can be obtained by applying the operator equations (2) to $\mathcal{H}_{\text{int}}$. By carrying out this lengthy procedure the following forms for the D_{ij} matrices are obtained

$$D_{11} = D_{22} = \begin{pmatrix} a_{11} & 0 & a_{13} \\ 0 & a_{22} & 0 \\ a_{13} & 0 & a_{33} \end{pmatrix},$$

$$D_{33} = D_{44} = \begin{pmatrix} a_{11} & 0 & -a_{13} \\ 0 & a_{22} & 0 \\ -a_{13} & 0 & a_{33} \end{pmatrix}$$

$$D_{12} = \begin{pmatrix} b_{11} & 0 & b_{13} \\ 0 & b_{22} & 0 \\ b_{13} & 0 & b_{33} \end{pmatrix}, \quad D_{34} = \begin{pmatrix} b_{11} & 0 & -b_{13} \\ 0 & b_{22} & 0 \\ -b_{13} & 0 & b_{33} \end{pmatrix} \tag{10}$$

$$D_{13} = D_{24} = \begin{pmatrix} c_{11} & 0 & c_{13} \\ 0 & c_{22} & 0 \\ -c_{13} & 0 & c_{33} \end{pmatrix},$$

$$D_{14} = D_{23} = \begin{pmatrix} d_{11} & 0 & d_{13} \\ 0 & d_{22} & 0 \\ -d_{13} & 0 & d_{33} \end{pmatrix}.$$

It can be seen that some of the interaction matrices are symmetric and that each of the other ones can be decomposed into a sum of a symmetrical matrix and an antisymmetrical one. The antisymmetrical part in each case can be written in the form of Dzyaloshinsky-Moriya antisymmetric exchange with a Dzyaloshinsky vector along the crystallographic $\vec{b}$ axis.

C. Spin configurations in the space group *Pbcn* [sites 4(c)]

Following the notation used by Bertaut,[6] we shall characterize the spin configurations of the four

Ni^{2+} ions in the crystallographic unit cell by specifying the nonzero components of the vectors $\vec{F}$, $\vec{G}$, $\vec{C}$, and $\vec{A}$ given by

$$\begin{aligned}\vec{F}&=\vec{S}_1+\vec{S}_2+\vec{S}_3+\vec{S}_4,\\ \vec{G}&=\vec{S}_1-\vec{S}_2+\vec{S}_3-\vec{S}_4,\\ \vec{C}&=\vec{S}_1+\vec{S}_2-\vec{S}_3-\vec{S}_4,\\ \vec{A}&=\vec{S}_1-\vec{S}_2-\vec{S}_3+\vec{S}_4.\end{aligned}\tag{11}$$

In order to find the spin configurations that preserve the space-group *Pbcn*, namely those in which the magnetic unit cell is identical to the crystallographic one, it is necessary to consider the time reversal operator. The elements of the space group are 1, 2_{1x}, 2_y, 2_{1z}, $\bar{1}$, $\bar{1}2_{1x}$, $\bar{1}2_y$, $\bar{1}2_{1z}$. The various isomorphic magnetic groups arise when the time reversal operator is either combined or not combined with each of the generators.

As each of the three generators can be either combined or not combined with the time reversal operator, there are eight possible spin configurations compatible with the maximal symmetry of the space group *Pbcn*. Since the time reversal operator only reverses the components of a spin, and the spin transformations under the generators of *Pbcn* are known (see Table I) it is easy to find out the transformation properties of the spins under any operator of the magnetic groups. When this is done, the eight spin configurations listed in Table II are obtained.

Note that the configurations in Table II are only those that have the magnetic unit cell identical to the crystallographic one. If this restriction is dropped then antiferromagnetic spin configurations are possible in which the unit cell is doubled along one or more of the orthorhombic axes. In that case each one of the configurations in Table II can be reversed after a translation by one lattice constant in the direction along which the unit cell is doubled. Such like configurations however, no longer possess the full symmetry of the space group *Pbcn*.

TABLE II. Spin configurations and magnetic groups in $Pbcn(\vec{k}=0)$ (primes indicate time reversal).

Spin configurations	Generators	Magnetic group
C_y	$2_{1x}2_y\bar{1}$	$Pbcn$
G_xA_z	$2_{1x}2'_y\bar{1}'$	$Pb'cn$
G_y	$2'_{1x}2_y\bar{1}'$	$Pbc'n$
G_zA_x	$2'_{1x}2'_y\bar{1}'$	$Pbcn'$
F_zC_x	$2'_{1x}2'_y\bar{1}$	$Pb'c'n$
F_xC_z	$2_{1x}2'_y\bar{1}$	$Pbc'n'$
F_y	$2'_{1x}2_y\bar{1}$	$Pb'cn'$
A_y	$2_{1x}2_y\bar{1}'$	$Pb'c'n'$

IV. ANALYSIS

The ground level of $Ni^{2+}(d^8)$ ions in an octahedral crystal field is $^3A_2$.[7] With other levels being thousands of degrees above the ground level[8] their population can be neglected at temperatures below room temperature. Their only contribution to the susceptibility is through a constant Van Vleck term which is found to be negligible in our temperature range of interest (see Fig. 1). Therefore only the Ni^{2+} ions occupying the ground level manifold will be considered. In $NiNb_2O_6$ the symmetry of the crystal field at the sites of the Ni^{2+} ions is less than octahedral, and therefore the degeneracy of the ground level will very likely be reduced. In the forthcoming analysis an effective spin Hamiltonian formalism with $S=1$ is employed to describe the behavior of the Ni^{2+} ions. The crystallographic $\vec{c}$ axis is taken to be the spin easy axis for all the Ni^{2+} spins and a two sublattice description of the Ni^{2+} spins in the mean-field approximation is adopted.

The effective spin Hamiltonian of the Ni^{2+} spins can be written in the form

$$\begin{aligned}\mathcal{H}=&\sum_{i_1,j_1}\vec{S}^t_{i_1}A_{11}\vec{S}_{j_1}+\sum_{i_2,j_2}\vec{S}^t_{i_2}A_{22}\vec{S}_{j_2}+\sum_{i_1,j_2}\vec{S}^t_{i_1}A_{12}\vec{S}_{j_2}\\ &-K\sum_l S^2_{lz}-\vec{H}\cdot\mu_B\sum_l g_l\cdot\vec{S}_l,\end{aligned}\tag{12}$$

where $\vec{S}_{i_1}$ and $\vec{S}_{j_1}$ are spins in one sublattice, $\vec{S}_{i_2}$ and $\vec{S}_{j_2}$ belong to the other sublattice, $\vec{S}_l$ belongs to either one of the sublattices, the l summation extends over all spins and the i_k, j_n summations extend over pairs of interacting neighbor spins. The first two terms are Ni^{2+}-Ni^{2+} bilinear interactions within each sublattice. The third term is the bilinear interaction between Ni^{2+} spins on different sublattices. The magnetocrystalline anisotropy, which is taken to be uniaxial, is expressed in the fourth term. The last term is the direct interaction of the Ni^{2+} spins with the external magnetic field.

We take the Ni^{2+}-Ni^{2+} interaction matrices to be diagonal

$$A_{11}=A_{22}=\begin{pmatrix}y_{11}&0&0\\0&y_{22}&0\\0&0&y_{33}\end{pmatrix},\quad A_{12}=\begin{pmatrix}y'_{11}&0&0\\0&y'_{22}&0\\0&0&y'_{33}\end{pmatrix}.\tag{13}$$

With the local principal axes of the g tensor taken

to coincide with the crystallographic axes, the g matrices assume the following form:

$$g_1 = g_2 = \begin{pmatrix} g_x & 0 & 0 \\ 0 & g_y & 0 \\ 0 & 0 & g_z \end{pmatrix}. \tag{14}$$

The Hamiltonian (12) can be reduced to a more convenient form

$$\begin{aligned}\mathcal{H} = {} & z_{11}\langle\vec{S}_1^t\rangle A_{11}\sum_{j_1}\vec{S}_{j_1} + z_{22}\langle\vec{S}_2^t\rangle A_{22}\sum_{j_2}\vec{S}_{j_2} \\ & + \tfrac{1}{2} z_{21}\langle\vec{S}_1^t\rangle A_{12}\sum_{j_2}\vec{S}_{j_2} \\ & + \tfrac{1}{2} z_{12}\langle\vec{S}_2^t\rangle A_{12}^t\sum_{j_1}\vec{S}_{j_1} - K\sum_{j_1} S_{j_1 z}^2 \\ & - K\sum_{j_2} S_{j_2 z}^2 - \vec{H}\mu_B\sum_{j_1} g_1\vec{S}_{j_1} - \vec{H}\mu_B\sum_{j_2} g_2\vec{S}_{j_2},\end{aligned} \tag{15}$$

where z_{kl} is the effective number of interacting l-type neighbor spins of a k-type Ni^{2+} spin (note that $z_{11} = z_{22}$ and $z_{12} = z_{21}$) and $\langle\rangle$ indicates the thermal average. In the absence of an external field the ordered magnetic configuration has its antiferromagnetic axis along the $\vec{c}$ direction.

$$\begin{aligned}&\langle S_{1x}\rangle_0 = \langle S_{2x}\rangle_0 = 0, \quad \langle S_{1y}\rangle_0 = \langle S_{2y}\rangle_0 = 0, \\ &\langle S_{1z}\rangle_0 = -\langle S_{2z}\rangle_0.\end{aligned} \tag{16}$$

The perpendicular and parallel susceptibilities will now be calculated.

A. Perpendicular susceptibilities χ_a, χ_b

The Hamiltonian $\mathcal{H}$ of Eq. (15) is an effective Hamiltonian of decoupled spins where the Hamiltonian $\mathcal{H}_i$ of each spin in the spontaneously ordered configuration with an external field in the $\vec{a}$ direction is given by the expressions

$$\begin{aligned}\mathcal{H}_1 = {} & z_{11}\langle S_{1x}\rangle y_{11} S_{1x} + z_{11}\langle S_{1z}\rangle y_{33} S_{1z} \\ & + \tfrac{1}{2} z_{12}\langle S_{2x}\rangle y'_{11} S_{1x} + \tfrac{1}{2} z_{12}\langle S_{2z}\rangle y'_{33} S_{1z} \\ & - K S_{1z}^2 - g_x\mu_B H S_{1x}, \\ \mathcal{H}_2 = {} & z_{22}\langle S_{2x}\rangle y_{11} S_{2x} + z_{22}\langle S_{2z}\rangle y_{33} S_{2z} \\ & + \tfrac{1}{2} z_{21}\langle S_{1x}\rangle y'_{11} S_{2x} + \tfrac{1}{2} z_{21}\langle S_{1z}\rangle y'_{33} S_{2z} \\ & - K S_{2z}^2 - g_x\mu_B H S_{2x}.\end{aligned} \tag{17}$$

The spin components are now expanded in powers of H and retaining only terms up to the first order in H at low fields one has

$$\begin{aligned}&\langle S_{1x}\rangle = a'_1 H, \quad \langle S_{2x}\rangle = a'_2 H, \quad \langle S_{1y}\rangle = \langle S_{2y}\rangle = 0, \\ &\langle S_{1z}\rangle = \langle S_{1z}\rangle_0, \quad \langle S_{2z}\rangle = -\langle S_{1z}\rangle_0.\end{aligned} \tag{18}$$

By using these expansions, $\mathcal{H}_1$ and $\mathcal{H}_2$ assume the following forms:

$$\mathcal{H}_1 = \mathcal{H}_{10} + \mathcal{H}'_1, \quad \mathcal{H}_2 = \mathcal{H}_{20} + \mathcal{H}'_2, \tag{19}$$

where

$$\begin{aligned}\mathcal{H}_{10} &= (z_{11}y_{33} - \tfrac{1}{2} z_{12}y'_{33})\langle S_{1z}\rangle_0 S_{1z} - K S_{1z}^2, \\ \mathcal{H}'_1 &= (z_{11}y_{11}a'_1 + \tfrac{1}{2} z_{12}y'_{11}a'_2 - g_x\mu_B) H S_{1x}, \\ \mathcal{H}_{20} &= (z_{22}y_{33} - \tfrac{1}{2} z_{21}y'_{33})\langle S_{2z}\rangle_0 S_{2z} - K S_{2z}^2, \\ \mathcal{H}'_2 &= (z_{22}y_{11}a'_2 + \tfrac{1}{2} z_{21}y'_{11}a'_1 - g_x\mu_B) H S_{2x}.\end{aligned} \tag{20}$$

The unperturbed energy levels are given by

$$E_{1m} = E_{2m} = (z_{11}y_{33} - \tfrac{1}{2} z_{12}y'_{33})\langle S_{1z}\rangle_0 m - K m^2. \tag{21}$$

The matrix elements of S_{1z} and S_{1x} in the scheme of the eigenfunctions $|m\rangle$ of S_{1z} are given by the ordinary expressions

$$\begin{aligned}&(S_{1z})_{mm'} = m\delta_{mm'}, \\ &(S_{1x})_{mm'} = \tfrac{1}{2}[S(S+1) - mm']^{1/2}\delta_{m', m\pm 1}.\end{aligned} \tag{22}$$

$\langle S_{1x}\rangle$ is evaluated using the formula

$$\langle S_{1x}\rangle = \sum_{m,m'} (e^{-\mathcal{H}_1/kT})_{mm'} (S_{1x})_{m'm} \Big/ \sum_m (e^{-\mathcal{H}_1/kT})_{mm}. \tag{23}$$

The operator $e^{-\mathcal{H}_1/kT}$ will be expanded up to the first order in $\mathcal{H}'_1$ in terms of matrix elements. As

$$\mathcal{H}_1 = \mathcal{H}_{10} + \mathcal{H}'_1, \quad \mathcal{H}'_1 \ll \mathcal{H}_{10}, \quad \text{and} \quad [\mathcal{H}'_1, \mathcal{H}_{10}] \neq 0, \tag{24}$$

the expansion assumes the form[9]

$$e^{-\mathcal{H}_1/kT} \approx e^{-\mathcal{H}_{10}/kT} - \frac{1}{kT} e^{-\mathcal{H}_{10}/kT} \int_0^1 d\lambda e^{+\lambda\mathcal{H}_{10}/kT} \mathcal{H}'_1 e^{-\lambda\mathcal{H}_{10}/kT}. \tag{25}$$

When the integration is carried out one has

$$(e^{-\mathcal{H}_1/kT})_{mm'} \approx e^{-E_{1m}/kT}\delta_{mm'} - \frac{1}{kT} e^{-E_{1m}/kT}(\mathcal{H}'_1)_{mm'}\delta(E_{1m}, E_{1m'}) + \frac{e^{-E_{1m}/kT} - e^{-E_{1m'}/kT}}{E_{1m} - E_{1m'}}(\mathcal{H}_1)_{mm'}[1 - \delta(E_{1m}, E_{1m'})], \tag{26}$$

where

$$\delta(E_i, E_j) = \begin{cases} 1, & E_i = E_j, \\ 0, & E_i \neq E_j. \end{cases} \tag{27}$$

$(\mathcal{H}_1')_{mm'}$ to be used in this formula is easily evaluated as

$$(\mathcal{H}_1')_{mm'} = (z_{11}y_{11}a_1' + \tfrac{1}{2}z_{12}y_{11}'a_2' - g\mu_B)H\ \tfrac{1}{2}[S(S+1) - mm']^{1/2}\delta_{m'm\pm1}. \tag{28}$$

Turning to Eq. (23), an expansion up to the first power of $\mathcal{H}_1'$ yields the following expression (when only the first power of H is retained)

$$\langle S_{1x}\rangle = \tfrac{1}{4}(z_{11}y_{11}a_1' + \tfrac{1}{2}z_{12}y_{11}'a_2' - g_x\mu_B)\sum_m \Bigg(\frac{e^{-E_{1m}/kT} - e^{-E_{1m+1}/kT}}{-(z_{11}y_{33} - \tfrac{1}{2}z_{12}y_{33}')\langle S_{1z}\rangle_0 + 2mK + K}[S(S+1) - m(m+1)]$$
$$+ \frac{e^{-E_{1m}/kT} - e^{-E_{1m-1}/kT}}{(z_{11}y_{33} - \tfrac{1}{2}z_{12}y_{33}')\langle S_{1z}\rangle_0 - 2mK + K}[S(S+1) - m(m-1)]\Bigg)H\Bigg(\sum_m e^{-E_{1m}/kT}\Bigg)^{-1}. \tag{29}$$

When this expression is compared to the expansion $\langle S_{1x}\rangle = a_1'H$, one gets an equation in which a_1' and a_2' are involved. Due to the symmetry of the problem one has $a_1' = a_2'$ and therefore a_1' can be evaluated.

The susceptibility χ_a in the $\vec{a}$ direction will be given by the formula

$$\chi_a = Ng_x\mu_B a_1'. \tag{30}$$

When the expression for a_1' is used one obtains the formula for the $\vec{a}$ susceptibility in the temperature range below T_N,

$$\chi_a(T) = Ng_x^2\mu_B^2\Bigg\{(z_{11}y_{11} + \tfrac{1}{2}z_{12}y_{11}')$$
$$- 4\Bigg(\sum_{m=-S}^{S} e^{-E_{1m}/kT}\Bigg)\Bigg[\sum_{m=-S}^{S-1}\Bigg(\frac{e^{-E_{1m}/kT} - e^{-E_{1m+1}/kT}}{-(z_{11}y_{33} - \tfrac{1}{2}z_{12}y_{33}')\langle S_{1z}\rangle_0 + 2mK + K}[S(S+1) - m(m+1)]\Bigg)$$
$$+ \sum_{m=-(S-1)}^{S}\Bigg(\frac{e^{-E_{1m}/kT} - e^{-E_{1m-1}/kT}}{(z_{11}y_{33} - \tfrac{1}{2}z_{12}y_{33}')\langle S_{1z}\rangle_0 - 2mK + K}[S(S+1) - m(m-1)]\Bigg)\Bigg]^{-1}\Bigg\}^{-1}. \tag{31}$$

It can be seen that at $T = 0$ K one has

$$\chi_a(T = 0\text{ K}) = Ng_x^2\mu_B^2[(z_{11}y_{11} + \tfrac{1}{2}z_{12}y_{11}') - (z_{11}y_{33} - \tfrac{1}{2}z_{12}y_{33}') + 2K - (K/S)]^{-1}. \tag{32}$$

Formula (31) can be used also to derive χ_a in the temperature range $T_N \leq T$. To this end, expansions in powers of $(E_{1m} - E_{1m\pm1})/kT$ are sometimes used when $|K/kT_N| \ll 1$.[10] When T_N is low this is unlikely to be the case and therefore this method will not be followed here. Instead, one can put $\langle S_{1z}\rangle_0 = 0$ in formula (31) to obtain the susceptibility in the temperature range $T_N \leq T$ resulting in the expression

$$\chi_a(T) = Ng_x^2\mu_B^2\Bigg\{(z_{11}y_{11} + \tfrac{1}{2}z_{12}y_{11}') - 4\Bigg(\sum_{m=-S}^{S} e^{Km^2/kT}\Bigg)\Bigg[\sum_{m=-S}^{S-1}\Bigg(\frac{e^{Km^2/kT}(1 - e^{(2mK+K)/kT})}{2mK + K}[S(S+1) - m(m+1)]\Bigg)$$
$$+ \sum_{m=-(S-1)}^{S}\Bigg(\frac{e^{Km^2/kT}(1 - e^{(-2mK+K)/kT})}{-2mK + K}[S(S+1) - m(m-1)]\Bigg)\Bigg]^{-1}\Bigg\}^{-1}. \tag{33}$$

The susceptibility along the crystallographic $\vec{b}$ axis is obtained when g_x and $(z_{11}y_{11} + \frac{1}{2}z_{12}y_{11}')$ are replaced by g_y and $(z_{11}y_{22} + \frac{1}{2}z_{12}y_{22}')$, respectively, in formulas (31), (32), and (33).

B. Parallel susceptibility χ_c

The Hamiltonian $\mathcal{H}_i$ of each spin in the spontaneously ordered configuration with an external field

in the $\vec{c}$ direction is given by the expressions

$$\mathcal{H}_1 = z_{11}\langle S_{1z}\rangle y_{33}S_{1z} + \tfrac{1}{2}z_{12}\langle S_{2z}\rangle y'_{33}S_{1z} - KS_{1z}^2 - g_z\mu_B HS_{1z},$$
$$\mathcal{H}_2 = z_{22}\langle S_{2z}\rangle y_{33}S_{2z} + \tfrac{1}{2}z_{21}\langle S_{1z}\rangle y'_{33}S_{2z} - KS_{2z}^2 - g_z\mu_B HS_{2z}, \quad (34)$$

for sublattices 1 and 2, respectively.

To proceed we expand $\langle S_{iz}\rangle$ in powers of H and retain terms up to the first power only at low fields

$$\langle S_{1z}\rangle = \langle S_{1z}\rangle_0 + c'_1H, \quad \langle S_{2z}\rangle = -\langle S_{1z}\rangle_0 + c'_2H. \quad (35)$$

$\langle S_{iz}\rangle$ is given by

$$\langle S_{iz}\rangle = \mathrm{Tr}(e^{-\mathcal{H}_i/kT}S_{iz})/\mathrm{Tr}(e^{-\mathcal{H}_i/kT}), \quad i=1,2, \quad (36)$$

where

$$\begin{aligned}\mathcal{H}_1 &= z_{11}(\langle S_{1z}\rangle_0 + c'_1H)y_{33}S_{1z} + \tfrac{1}{2}z_{12}(-\langle S_{1z}\rangle_0 + c'_2H)y'_{33}S_{1z} - KS_{1z}^2 - g_z\mu_BHS_{1z}\\ &= (z_{11}y_{33} - \tfrac{1}{2}z_{12}y'_{33})\langle S_{1z}\rangle_0S_{1z} - KS_{1z}^2 + (c'_1z_{11}y_{33} + \tfrac{1}{2}c'_2z_{12}y'_{33} - g_z\mu_B)HS_{1z},\\ \mathcal{H}_2 &= z_{22}(\langle S_{2z}\rangle_0 + c'_2H)y_{33}S_{2z} + \tfrac{1}{2}z_{21}(-\langle S_{2z}\rangle_0 + c'_1H)y'_{33}S_{2z} - KS_{2z}^2 - g_z\mu_BHS_{2z}\\ &= (z_{22}y_{33} - \tfrac{1}{2}z_{21}y'_{33})\langle S_{2z}\rangle_0S_{2z} - KS_{2z}^2 + (c'_2z_{22}y_{33} + \tfrac{1}{2}c'_1z_{21}y'_{33} - g_z\mu_B)HS_{2z}.\end{aligned} \quad (37)$$

Substitution of $\mathcal{H}_1$ in (36) gives

$$\langle S_{1z}\rangle = \frac{\sum_m (e^{-\mathcal{H}_1/kT})_{mm}(S_{1z})_{mm}}{\sum_m (e^{-\mathcal{H}_1/kT})_{mm}} \approx \frac{\sum_m e^{-E_{1m}/kT}m\left[1 - \frac{1}{kT}(c'_1z_{11}y_{33} + \frac{1}{2}c'_2z_{12}y'_{33} - g_z\mu_B)Hm\right]}{\sum_m e^{-E_{1m}/kT}\left[1 - \frac{1}{kT}(c'_1z_{11}y_{33} + \frac{1}{2}c'_2z_{12}y'_{33} - g_z\mu_B)Hm\right]}$$
$$\approx \langle S_{1z}\rangle_0 + \frac{1}{kT}(c'_1z_{11}y_{33} + \tfrac{1}{2}c'_2z_{12}y'_{33} - g_z\mu_B)(\langle S_{1z}\rangle_0^2 - \langle S_{1z}^2\rangle_0)H. \quad (38)$$

Comparing this with the expansion $\langle S_{1z}\rangle = \langle S_{1z}\rangle_0 + c'_1H$ one has

$$c'_1 = (1/kT)(c'_1z_{11}y_{33} + \tfrac{1}{2}c'_2z_{12}y'_{33} - g_z\mu_B)(\langle S_{1z}\rangle_0^2 - \langle S_{1z}^2\rangle_0). \quad (39)$$

Similarly, from Eqs. (36) and (37) it follows that

$$\langle S_{2z}\rangle \approx -\langle S_{1z}\rangle_0 + (1/kT)(c'_2z_{22}y_{33} + \tfrac{1}{2}c'_1z_{21}y'_{33} - g_z\mu_B) \times (\langle S_{1z}\rangle_0^2 - \langle S_{1z}^2\rangle_0)H. \quad (40)$$

When this is compared to the expansion $\langle S_{2z}\rangle = -\langle S_{1z}\rangle_0 + c'_2H$ one gets

$$c'_2 = (1/kT)(c'_2z_{22}y_{33} + \tfrac{1}{2}c'_1z_{21}y'_{33} - g_z\mu_B)(\langle S_{1z}\rangle_0^2 - \langle S_{1z}^2\rangle_0). \quad (41)$$

From Eqs. (39) and (41) the expressions for c'_1 and c'_2 are obtained

$$c'_1 = c'_2 = \frac{g_z\mu_B(\langle S_{1z}^2\rangle_0 - \langle S_{1z}\rangle_0^2)}{kT + (z_{11}y_{33} + \frac{1}{2}z_{12}y'_{33})(\langle S_{1z}^2\rangle_0 - \langle S_{1z}\rangle_0^2)}. \quad (42)$$

This yields the susceptibility χ_c in the $\vec{c}$ direction in the temperature range $T < T_N$,

$$\chi_c = \tfrac{1}{2}N(c'_1 + c'_2)g_z\mu_B$$

or

$$\chi_c = \frac{Ng_z^2\mu_B^2(\langle S_{1z}^2\rangle_0 - \langle S_{1z}\rangle_0^2)}{kT + (z_{11}y_{33} + \frac{1}{2}z_{12}y'_{33})(\langle S_{1z}^2\rangle_0 - \langle S_{1z}\rangle_0^2)}. \quad (43)$$

It can be shown that $\chi_c(T=0\text{ K}) = 0$.

In order to find the temperature dependence of χ_c close to T_N, the expressions for $\langle S_{1z}\rangle_0$ and $\langle S_{1z}^2\rangle_0$ in the temperature range close to T_N will be obtained

$$\langle S_{1z}\rangle_0 = \sum_m \exp\left(\frac{1}{kT}[(\tfrac{1}{2}z_{12}y'_{33} - z_{11}y_{33})\langle S_{1z}\rangle_0m + Km^2]\right)m\left[\sum_m \exp\left(\frac{1}{kT}[(\tfrac{1}{2}z_{12}y'_{33} - z_{11}y_{33})\langle S_{1z}\rangle_0m + Km^2]\right)\right]^{-1}. \quad (44)$$

Close to T_N $\langle S_{1z}\rangle_0$ is small and expansion of the exponents up to the third power of $\langle S_{1z}\rangle_0$ yields the relation

$$\langle S_{1z}\rangle_0^2 = \frac{6[kT - (\frac{1}{2}z_{12}y'_{33} - z_{11}y_{33})F_2(kT)](kT)^2}{(\frac{1}{2}z_{12}y'_{33} - z_{11}y_{33})^2[(\frac{1}{2}z_{12}y'_{33} - z_{11}y_{33})F_4(kT) - 3kTF_2(kT)]}, \quad (45)$$

where

$$F_l(kT) = \sum_m e^{Km^2/kT}m^l \Big/ \sum_m e^{Km^2/kT}. \quad (46)$$

The transition temperature T_N is determined by the requirement that at T_N $\langle S_{1z}\rangle_0 = 0$. Therefore

$$kT_N = (\tfrac{1}{2}z_{12}y'_{33} - z_{11}y_{33})F_2(kT_N)\,. \tag{47}$$

Taking

$$\langle S^2_{1z}\rangle_0 = \sum_m \exp\left(\frac{1}{kT}[(\tfrac{1}{2}z_{12}y'_{33} - z_{11}y_{33})\langle S_{1z}\rangle_0 m + Km^2]\right) m^2 \left[\sum_m \exp\left(\frac{1}{kT}[(\tfrac{1}{2}z_{12}y'_{33} - z_{11}y_{33})\langle S_{1z}\rangle_0 m + Km^2]\right)\right]^{-1}, \tag{48}$$

an expansion up to the third power of $\langle S_{1z}\rangle_0$ close to T_N yields

$$\langle S^2_{1z}\rangle_0 = F_2(kT) + \tfrac{1}{2}[1/(kT)^2](\tfrac{1}{2}z_{12}y'_{33} - z_{11}y_{33})^2 \times [F_4(kT) - F_2(kT)^2]\langle S_{1z}\rangle_0^2\,. \tag{49}$$

At $T = T_N$,

$$\langle S^2_{1z}\rangle_0 = F_2(kT_N)\,,$$

so that one has

$$\chi_c(T = T_N) = Ng_z^2\mu_B^2/2(\tfrac{1}{2}z_{12}y'_{33})\,. \tag{50}$$

Formula (43) can be used also to derive χ_c in the temperature range $T_N \leq T$. This is done by putting $\langle S_{1z}\rangle_0 = 0$ in formulas (48) and (43).

C. Experimental data and determination of parameters

The various parameters involved in the theoretical formulas were deduced from the measured susceptibility curves in the temperature range 1.4–300 K (Fig. 1). The experimental data have been corrected for demagnetization and normalized to correspond to a zero demagnetization factor. Demagnetization corrections however were small, never exceeding 5% of the measured values. We fitted formulas (31), (33), and (43) to the experimental susceptibility data. As some of the parameters are shared by two formulas or more, a least squares technique was employed to fit all sets of data simultaneously. The following results were obtained

$$\begin{aligned}
&z_{11}y_{11} + \tfrac{1}{2}z_{12}y'_{11} = (-0.73 \pm 0.10)\times 10^{-15}[\text{erg/spin}] \\
&\qquad = -5.3 \pm 0.7[\text{K/spin}]\,, \\
&z_{11}y_{22} + \tfrac{1}{2}z_{12}y'_{22} = (-1.0 \pm 0.1)\times 10^{-15}[\text{erg/spin}] \\
&\qquad = -7.3 \pm 0.7[\text{K/spin}]\,, \\
&z_{11}y_{33} = (-0.68 \pm 0.10)\times 10^{-15}[\text{erg/spin}] \\
&\qquad = -4.9 \pm 0.7[\text{K/spin}]\,, \\
&\tfrac{1}{2}z_{12}y'_{33} = (0.35 \pm 0.10)\times 10^{-15}[\text{erg/spin}] \\
&\qquad = 2.5 \pm 0.7[\text{K/spin}]\,, \\
&g_x = g_y = g_z = g = 2.4 \pm 0.1\,, \\
&K = (10.9 \pm 1.0)\times 10^{-16}[\text{erg/spin}] \\
&\quad = 7.9 \pm 0.7[\text{K/spin}]\,.
\end{aligned} \tag{51}$$

The quoted errors are statistical and indicate two standard deviations. The g tensor was set in advance to be isotropic since the possible low anisotropy in the g tensor that Ni^{2+} ions often exhibit[11] would very likely fall within the statistical error. In the derivation of the parameters it was taken into account that the sensitivity of the least-squares fit to some of the parameters is dependent on the temperature range over which the fit is done. It is for this reason that the magnetocrystalline uniaxial anisotropy parameter K was determined solely from the susceptibility data in the temperature range below T_N. The least-squares fit was not so sensitive to K values at higher temperatures. g was deduced from susceptibility data in the temperature range above T_N and was found to agree very well with that obtained from magnetization vs field curves in the $\vec{a}-\vec{c}$ plane at $T = 1.4$ K (not shown). In determining the Ni^{2+}-Ni^{2+} bilinear interaction parameters the experimental susceptibility in the whole range 1.4–300 K was considered in the least-squares fit. Good agreement is found between susceptibility curves calculated with the parameters (51) and the experimental data (see Fig. 1).

Calculation of T_N using formula (47) with parameters (51) yields $T_N = 6.5$ K, which is slightly higher than the ordering temperature associated with the maximum in $d\chi/dT$.

It is evident from the parameters (51) that along all three crystallographic directions the dominant coupling between Ni^{2+} spins is the ferromagnetic intrasublattice coupling rather than the antiferromagnetic intersublattice interaction. By using Hamiltonian (17) and the parameters (51) we calculated the Ni^{2+}-Ni^{2+} effective fields at $T = 0$ K in the spontaneously ordered configuration

$$\begin{aligned}
H^{\text{f}}_{11c} = H^{\text{f}}_{22c} &= \left|\frac{z_{11}y_{33}S}{g_z\mu_B}\right| = 30.7 \pm 5.5[\text{kOe}]\,, \\
H^{\text{af}}_{21c} = H^{\text{af}}_{12c} &= \left|\frac{\tfrac{1}{2}z_{12}y'_{33}S}{g_z\mu_B}\right| = 15.6 \pm 5.0[\text{kOe}]\,.
\end{aligned} \tag{52}$$

The H^{f}_{iic} and $H^{\text{af}}_{ijc}(i \neq j)$ are the magnitudes of the ferromagnetic intrasublattice and the antiferromagnetic intersublattice fields, respectively,

in the spontaneously ordered configuration at $T=0$ K. The total Ni^{2+}-Ni^{2+} effective field H_{Ni}^{eff} at $T=0$ K is

$$H_{Ni}^{eff}=H_{11c}^{f}+H_{12c}^{af}=46.3\pm10.5[\text{kOe}]. \quad (53)$$

In H_{Ni}^{eff} both exchange and dipolar contributions are included. Similarly, the magnitudes of the Ni^{2+}-Ni^{2+} effective fields H_{aNi}^{eff}, H_{bNi}^{eff} and H_{cNi}^{eff} in the field induced paramagnetic configurations along the three crystallographic directions $\vec{a}$, $\vec{b}$, $\vec{c}$, respectively, at $T=0$ K are given by

$$H_{aNi}^{eff}=\left|\frac{(z_{11}y_{11}+\frac{1}{2}z_{12}y'_{11})S}{g_x\mu_B}\right|=32.8\pm5.6[\text{kOe}],$$

$$H_{bNi}^{eff}=\left|\frac{(z_{11}y_{22}+\frac{1}{2}z_{12}y'_{22})S}{g_y\mu_B}\right|=45.4\pm6.4[\text{kOe}], \quad (54)$$

$$H_{cNi}^{eff}=H_{11c}^{eff}-H_{12c}^{eff}=15.1\pm10.5[\text{kOe}].$$

H_{aNi}^{eff}, H_{bNi}^{eff}, and H_{cNi}^{eff} give the net ferromagnetic coupling in the configurations in question. Without knowing the detailed spin configuration of $NiNb_2O_6$ we were in no position to calculate the Ni^{2+}-Ni^{2+} dipolar fields in the spontaneously ordered structure. However, it is possible to derive the Ni^{2+}-Ni^{2+} dipolar fields in the various field-induced paramagnetic spin configurations since in these the magnetic unit cell is identical to the crystallographic one. We calculated the dipolar parts of the Ni^{2+}-Ni^{2+} effective fields (54) taking a magnetic moment of $2.4\mu_B$ per Ni^{2+} ion. One has

$$H_{aNi\,dip}^{eff}=-2.6[\text{kOe}],$$

$$H_{bNi\,dip}^{eff}=-0.5[\text{kOe}], \quad (55)$$

$$H_{cNi\,dip}^{eff}=3.0[\text{kOe}],$$

where (–) signs indicate dipolar fields in opposite direction to the Ni^{2+} magnetic moments. It is evident that exchange interactions constitute the dominant part of the Ni^{2+}-Ni^{2+} bilinear coupling.

In the analysis developed here the magnetocrystalline anisotropy has been incorporated in the expression for the Ni^{2+} single-ion energy levels [see Eq. (21)]. We calculated the temperature dependence of these levels (Fig. 5) using Eqs. (21) and (44) with parameters (51). Sometimes however, when a different approach is adopted, the magnetocrystalline anisotropy in the mean-field approximation is expressed in terms of an effective anisotropy field H_K.[12] Using parameters (51), the anisotropy field at $T=0$ K is given by

$$H_K(T=0\text{ K})=2KS/g_z\mu_B=98.0\pm12.7[\text{kOe}]. \quad (56)$$

H_K is thus higher in magnitude than the Ni^{2+}-Ni^{2+} effective fields in the material. Acting along the antiferromagnetic axis in the direction of the magnetization on each sublattice, the magnetocrystalline anisotropy field has a remarkable effect on the magnitude of the sublattice magnetization. We applied an iteration method on Eq. (44) and calculated the temperature dependence of the normalized sublattice magnetization using parameters (51). For comparison, we repeated the calculations for the case $K=0$ and it is clearly demonstrated that the presence of the magnetocrystalline anisotropy can result in a substantial additional polarization of the spins (see Fig. 6). The remarkable decrease in the susceptibility along all three principal crystallographic directions below T_N is due in fact to the relatively high uniaxial anisotropy.

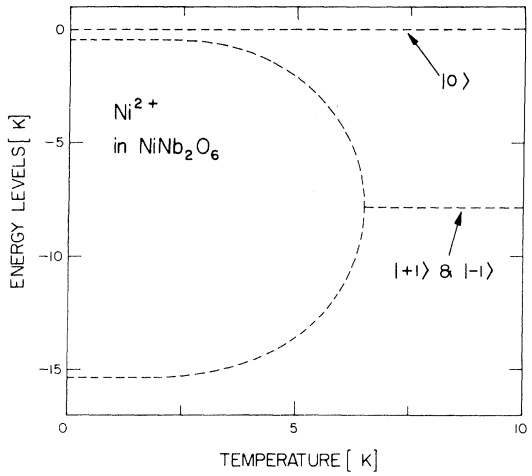

FIG. 5. Calculated temperature dependence of the Ni^{2+} energy levels of the ground term $^3A_2$ in $NiNb_2O_6$ using the parameters derived in the text.

V. DISCUSSION

In this paper, we have shown that the main features of the magnetic behavior of $NiNb_2O_6$ below

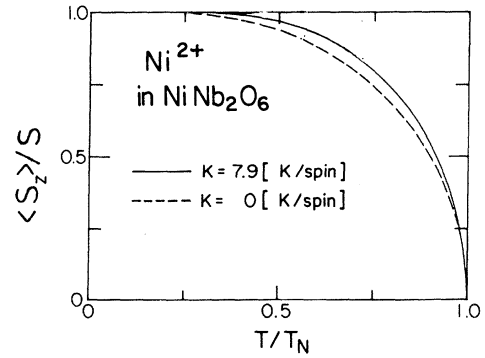

FIG. 6. Calculated temperature dependence of $\langle S_z\rangle/S$ for Ni^{2+} in $NiNb_2O_6$ for $K=7.9$ K/spin and $K=0$ K/spin using the parameters derived in the text.

room temperature can be satisfactorily accounted for in the mean-field approximation assuming a two-sublattice uniaxial-antiferromagnet description for the Ni^{2+} spins in this material. The antiferromagnetic axis was taken to coincide with the crystallographic $\vec{c}$ direction. It can be easily seen in Table II that in the spin configurations in *Pbcn* that are associated with $\vec{k}=0$, and in any possible doubling of these configurations in the principal crystallographic directions, $\vec{c}$ and $\vec{a}$ components of spin modes can coexist. The existence of nonzero $\vec{a}$ components in the presence of $\vec{c}$ components in these configurations implies a four sublattice structure in the $\vec{a}-\vec{c}$ plane in the case of an antiferromagnet. Thus the possibility of the Ni^{2+} spins forming a four sublattice rather than a two sublattice configuration in which the directions of the spins are close to, but do not coincide with the crystallographic $\vec{c}$ axis, cannot be ruled out.

The Ni^{2+}-Ni^{2+} bilinear interactions in this material are essentially of an exchange type with a small dipolar contribution. Along all three principal crystallographic directions we found the Ni^{2+}-Ni^{2+} intrasublattice ferromagnetic coupling to be stronger than the antiferromagnetic intersublattice interaction. We took the magnetocrystalline anisotropy to be uniaxial in the analysis of the experimental data. Information on some other Ni^{2+} materials[13] indicates that this rather arbitrary choice of the type of magnetocrystalline anisotropy need not necessarily be true. However, lacking an independent determination of the positions of the crystal-field levels of Ni^{2+} in $NiNb_2O_6$ we did not feel that anything was to be gained by taking a more general form of magnetocrystalline anisotropy [see relations (7)] even though introduction of more parameters could have improved the fit to $\chi_a(T)$ and $\chi_b(T)$ in the temperature range below T_N. The value of the over all splitting of the ground term $^3A_2$ that we obtained in $NiNb_2O_6$ is comparable to the $^3A_2$ splitting in some other Ni^{2+} compounds.[13] Contrary to the minor effect that the magnetocrystalline anisotropy has on the magnitude of the sublattice magnetization in materials with high T_N,[14] it is evident (see Fig. 6) that in $NiNb_2O_6$ the presence of the magnetocrystalline anisotropy field can result in a remarkable additional polarization of the Ni^{2+} spins. The decrease in the susceptibility below T_N is also attributed to the relatively high magnetocrystalline anisotropy in this material. A g value of 2.4 ± 0.1 deduced from our least-squares fit also falls within the range of values typical of Ni^{2+} ions in many materials.[11]

The parameters (51) we obtained from the least-squares fit of the theoretical expressions to the experimental data yield a Neel temperature $T_N = 6.5$ K which is somewhat higher than the one found experimentally. This is probably due in part to the approximations inherent in the mean-field theory which is known to provide a reasonable description only of the main features of the magnetic behavior of a spin system.

In this paper, the magnetic properties of $NiNb_2O_6$ have been studied for the first time. Consequently, a relatively simple approach has been adopted in the analysis. A more detailed information on the ordered spin structure of this material can be obtained in neutron-diffraction studies of single crystals. Also, the temperature and field dependence of the Ni^{2+} energy levels can be directly checked by other techniques such as electron spin resonance and magnetooptical experiments to yield information on the Ni^{2+}-Ni^{2+} interaction as well as on the magnetocrystalline anisotropy and the g tensor. We are hoping to do some of these experiments in the future.

ACKNOWLEDGMENTS

The authors are very much indebted to Dr. D. Mukamel for useful suggestions and helpful discussions during the course of this work. Many thanks are due to Professor R. Hornreich, Professor S. Shtrikman, and Dr. I. Maartense for stimulating discussions and for comments on the manuscript.

---

*Present address: Dept. of Physics and Astronomy, University of Georgia, Athens, Ga., 30602.

[1]K. Brandt, Ark. Kemi Mineral Geol. 17A, No. 15, p. 1 (1943).
[2]H. Weitzel and S. Klein, Solid State Commun. 12, 113 (1973).
[3]H. Weitzel, Z. Anorg. Allg. Chem. 380, 119 (1971).
[4]L. M. Holmes, A. A. Ballman, and R. R. Hecker, Solid State Commun. 11, 409 (1972).
[5]I. Yaeger, A. H. Morrish, and B. M. Wanklyn, Twenty First Annual Conference on Magnetism and Magnetic Materials, Philadelphia, 1975 (Program 3E-2) (unpublished).
[6]E. F. Bertaut, Acta Crystallogr. A 24, 217 (1968).
[7]L. E. Orgel, J. Chem. Phys. 23, 1004 (1955).
[8]See, for instance, J. S. Griffith, *The Theory of Transition-Metal Ions* (Cambridge U. P., Cambridge, Mass., 1961), p. 286.
[9]Y. Tenenbaum, Ph.D. thesis (Weizmann Institute of Science, Rehovot, 1971) (unpublished).

[10]See, for instance, W. P. Wolf, Phys. Rev. 108, 1152 (1957).
[11]See, for instance, A. N. Holden, C. Kittel, and W. A. Yager, Phys. Rev. 75, 1943 (1949).
[12]See, for example, G. Gorodetsky, S. Shtrikman, Y. Tenenbaum, and D. Treves, Phys. Rev. 181, 823 (1969).
[13]Compare with T. Moriya, Phys. Rev. 117, 635 (1960), and references cited therein.
[14]See, for example, M. Eibschutz, S. Shtrikman, and D. Treves, Phys. Rev. 156, 562 (1967).